Tunnelling and Underground Space Technology 91 (2019) 102997

Contents lists available at ScienceDirect

Tunnelling and Underground Space Technology

journal homepage: www.elsevier.com/locate/tust

Energy performance and economic feasibility of energy segmental linings for subway tunnels

Benoît Cousin[a], Alessandro F. Rotta Loria[a,c,*], Andrew Bourget[b], Fabrice Rognon[b], Lyesse Laloui[a]

[a] Swiss Federal Institute of Technology in Lausanne, EPFL, Laboratory of Soil Mechanics, Lausanne, Switzerland
[b] CSD INGÉNIEURS SA, Lausanne, Switzerland
[c] GEOEG Engineering, Lausanne, Switzerland

A B S T R A C T

This study focuses on the analysis of the energy performance and economic feasibility of so-called tunnel energy segmental linings: an innovative technology that couples the structural support role of the tunnel lining with the heating-cooling role of the heat exchanger harvesting both shallow geothermal and aerothermal energies. The work is based on three-dimensional time-dependent thermo-hydraulic finite element analyses of a real case-study and presents a sensitivity investigation on the energy performance of energy segmental linings for a variation of the following design solutions: (i) pipe configuration, (ii) heat carrier fluid flow rate and (iii) pipe distance from the tunnel intrados. Selecting the smaller pipe diameter for a pipe layout perpendicular to the tunnel axis involves installing a configuration with the higher pipe length per segment and represents the optimal solution in terms of thermal power harvested per unit lining surface. Increasing the heat carrier fluid flow rate to increase the turbulence in pipes represents an effective approach to improve the energy performance, with a decreasing effectiveness for a successive increase of the heat carrier fluid flow rate. Decreasing the distance between the pipes from the tunnel intrados significantly improves the energy performance, with an increasing effectiveness for a successive increase of the heat carrier fluid flow rate. The previous design solutions markedly influence the capital investment and operation costs of thermal power plants resorting to energy tunnels. For the same site conditions but different design solutions, these plants may not be considered economically attractive, with the most profitable application that is not necessarily associated with the design involving the highest harvested thermal power via the geostructure. Based on the results of this research, energy segmental linings appear a breakthrough technology for the renewable energy supply of the built environment when properly analysed and designed.

1. Introduction

The building sector is the largest energy-consuming sector: it accounts for over one-third of the final energy consumption for hot water, space heating and space cooling purposes, and represents a major source of carbon dioxide emissions globally (IEA, 2013). Decreasing the environmental impact of buildings via technologies that harvest renewable energy sources is a crucial challenge for the sustainability of human activity. In this context, employing subsurface structures that couple a structural support role with a heating-cooling role of shallow geothermal heat exchangers in the form of so-called energy geostructures represents a major opportunity to provide renewable energy to the built environment.

New tunnels are increasingly excavated in urban areas with full face tunnel boring machines, which enable tunnel excavation in weak ground with a minimal risk of damaging existing structures. This process is achieved by laying a permanent support made of prefabricated concrete segments called segmental linings right after the “tail” of the boring machines, while pursuing the excavation process. Historically, conventional tunnel segmental linings have been made of reinforced concrete and have solely provided structural support. In recent years, the integration of pipes in tunnel linings with a heat carrier fluid that circulates into them has led to innovative energy segmental linings, with the novel feature of providing coupled structural support and renewable energy harvested from the underground in the form of energy tunnels. A growing interest in energy tunnels is being noted in the urban planning of developed and developing urban areas because this technology represents a renewable energy source for energy networks on a city scale.

In the city of Paris, France, the project ‘Grand Paris Express’ is incorporating the development of the transportation infrastructure of the future Grand Paris network through the retrofit of existing metro lines and the construction of new ones. With most of the lines built underground and 162 km of tracks excavated using full face tunnel boring machines, the ‘Grand Paris Express’ offers a major opportunity for implementing energy segmental linings. This implementation would follow one energy segmental lining project constructed with subsequent actual energy exploitation (Frodl et al., 2010), as well as other applications that explored the thermal activation of urban tunnels as energy tunnels (Nicholson et al., 2014; Barla et al., 2016).

* Corresponding author.
E-mail addresses: alessandro.rottaloria@epfl.ch, alessandro.rottaloria@geoeg.net (A.F. Rotta Loria).

https://doi.org/10.1016/j.tust.2019.102997
Received 22 November 2018; Received in revised form 29 May 2019; Accepted 8 June 2019

Energy tunnels are characterised by completely different static features as well as by a markedly larger heat transfer potential compared to the current, most widely applied type of energy geostructures; energy piles. The first feature relates to the different shape and structural role that characterises tunnels compared to piles. The second feature is related to the wider surface that characterises tunnels compared to piles, and in particular of having an interface with air in the underground built environment in addition to the interface with the ground that entirely characterises energy piles. The presence of one interface between energy tunnels and air, and another interface with porous materials such as soil or rock, allows the harvesting of both aerothermal and shallow geothermal energies through this technology. This feature makes the energy exploitation achievable through energy tunnels particularly flexible yet challenging, because different heat sources can be employed but a multitude of coupled phenomena govern the thermo-hydraulic behaviour and the energy performance of such technology. These phenomena typically include (i) heat and mass transfer dominated by convection in the built environment adjacent to the energy wall, (ii) heat transfer dominated by conduction within the filling material of the geostructure and across the wall of the pipes, (iii) heat and mass transfer dominated by convection within the pipes of the geostructure, and (iv) heat transfer dominated by conduction in the ground, unless a significant groundwater flow resulting in mass transfer also leads to a convection dominated heat transfer.

To address fundamental aspects of the thermo-hydraulic behaviour and energy performance of energy tunnels, an increasing amount of studies have been performed in recent years. The energy performance of energy segmental linings for a variation in the conditions that govern the heat and mass transfer phenomena characterising the ground has been investigated (Di Donna and Barla, 2016). The phenomena and interactions occurring between energy segmental linings and the underground built environment where air is present have been considered (Bourne-Webb et al., 2016; Bidarmaghz and Narsilio, 2018; Peltier et al., 2019). Comments on the influence of some design solutions applicable to energy segmental linings have also been proposed (Barla and Di Donna, 2018). However, a comprehensive analysis of the energy performance of tunnel energy segmental linings for different design solutions is unavailable until now, with consequent drawbacks for the understanding of the energy exploitation and economic potential of such technology.

Looking at the previous challenges, this paper focuses on the analysis of the thermo-hydraulic behaviour of tunnel energy segmental linings for a twofold purpose: (i) to address the energy performance of the considered technology for a variation of design solutions including the pipe configuration, the flow rate of the heat carrier fluid circulating in the pipes, and the pipe embedment from the tunnel intrados; and (ii) to assess the economic attractiveness and profitability of thermal power plants resorting to energy segmental linings depending on the considered design solutions, in addition to the thermally active tunnel length. To achieve the previous goals, this study is based on three-dimensional (3-D) thermo-hydraulic finite element analyses of a real case study referring to the project 'Grand Paris Express', as well as on the economic analysis and profitability assessment of the considered energy network.

In the following, the investigated problem is presented first. Next, the influence of design solutions on the energy performance of energy segmental linings is analysed. Then, the economic attractiveness of a thermal power plant resorting to the operation of an energy segmental lining is evaluated, considering the influence of different design solutions on the cost of the application. Finally, concluding remarks are summarised.

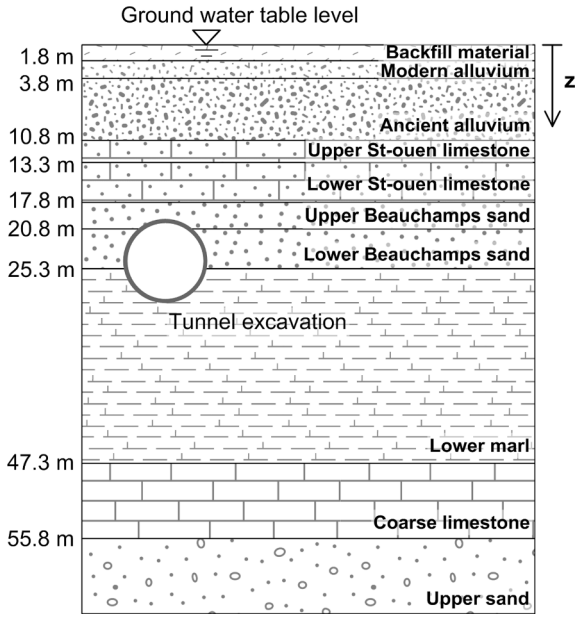

Fig. 1. Stratigraphic cross-section of the soil deposit encountered at the Chelles station.

2. Investigated problem

2.1. Grand Paris Express

In the framework of this study, the tunnel characteristics are those of the future line 16 of the project 'Grand Paris Express', with a focus on the typical geological conditions of the area of the Chelles station located in the east of Paris. The geological formations of the Parisian basin encountered during the tunnel excavation are mostly limestone and sands. The soil layers are fully saturated with water and are characterised by negligible groundwater flow (Société du Grand Paris, 2016). The schematic stratigraphic vertical cross-section of these formations is presented in Fig. 1.

2.2. Finite element model geometry

A 3-D finite-element model of the site is developed using the software COMSOL Multiphysics (COMSOL). The dimensions of this model are presented in Fig. 2.

The modelled tunnel has an outer diameter of D_{out} = 9.50 m and is excavated between depths of 19.7 m and 29.2 m. The tunnel is composed of a 40 cm-thick lining so that the inner diameter is of D_{in} = 8.70 m. The modelled lining ring is composed of six 4.20 m-long rectangular segments and one 3.40 m-long rectangular key. The breadth and height of the model domain are equal to ten times the external diameter of the tunnel, i.e., 95 m. This choice allows for avoiding ill-conditioning of the analyses results caused by boundary effects. The width of the model domain considers only a single 2 m-wide ring. This choice allows modelling an infinitely long tunnel via the use of symmetry planes detailed in Section 2.4. It has been considered to take advantage of the absence of groundwater flow along the axial direction of the tunnel.

The modelled tunnel is made of reinforced concrete and polyethylene pipes are embedded within the tunnel lining. The heat carrier fluid circulating in the pipes is water and the pipe configuration and its distance from the tunnel intrados are subjected to a sensitivity analysis detailed in Section 2.6.

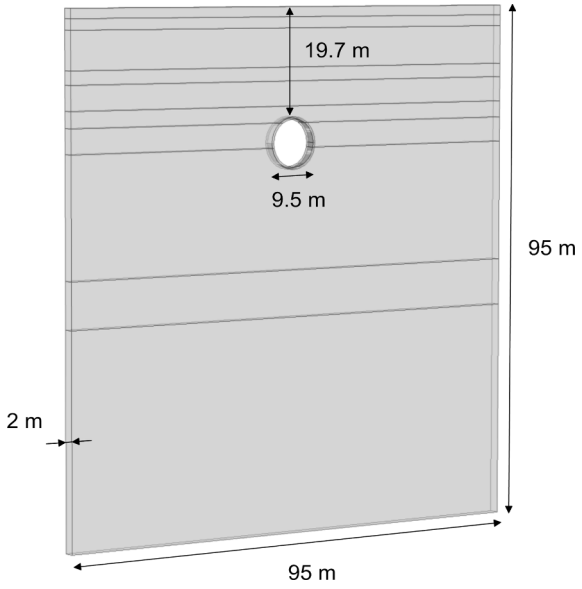

Fig. 2. Finite element model geometry.

2.3. Mathematical formulation

The following hypotheses are assumed to describe the thermo-hydraulic behaviour and the energy performance of the tunnel investigated in this study. Heat transfer by conduction characterises the ground, the filling material of the tunnel lining and the pipe walls. Heat transfer by convection and conduction characterises the heat carrier fluid circulating in the pipes. Heat transfer by convection characterises the interface between the tunnel and the air present in the underground built environment. To model the considered problem, time-dependent finite element analyses resorting to a thermo-hydraulic mathematical formulation are performed. The governing equations for fluid flow and heat transfer are coupled numerically.

The continuity and momentum conservation equations allowing to model the flow of an incompressible fluid within the pipes read, respectively:

$$\nabla\cdot(A_p\rho_f\bar{v}_{f,i}) = 0 \tag{1}$$

and

$$\rho_f\left(\frac{\partial\bar{v}_{f,i}}{\partial t}\right) = -\nabla p_f - f_D\frac{\rho_f}{2d_h}\,|\bar{v}_{f,i}|\,\bar{v}_{f,i} \tag{2}$$

where A_p [m²] is the inner cross-section of the pipe, ρ_f [kg/m³] is the heat carrier fluid density, $\bar{v}_{f,i}$ [m/s] is the average fluid velocity in the pipes, t [s] is the time, p_f [Pa] is the heat carrier fluid pressure, f_D [−] is the Darcy friction factor and d_h [m] is the hydraulic diameter of the pipe.

The energy conservation equation describing the convective–conductive heat transfer in the pipes for an incompressible fluid reads:

$$\rho_f A_p c_{p,f}\frac{\partial\bar{T}_f}{\partial t} + \rho_f A_p c_{p,f}\bar{v}_{f,i}\cdot\nabla\bar{T}_f = \nabla(A_p\lambda_f\nabla\bar{T}_f) + f_D\frac{\rho_f A_p}{2d_h}\,|\bar{v}_{f,i}|\,\bar{v}_{f,i}^2 + \dot{Q}_{wall} \tag{3}$$

with

$$\dot{Q}_{wall} = f(T_s, \bar{T}_f) \tag{4}$$

where $c_{p,f}$ [J/(kg°C)] and λ_f [W/(m°C)] are the specific heat and the thermal conductivity of the heat carrier fluid, respectively, and $\dot{Q}_{wall}$ [W/m] is the external heat exchange rate through the pipe wall. This latter term is a function of the temperature of the pipe wall T_s [°C] and the average temperature of the heat carrier fluid $\bar{T}_f$ [°C].

The energy conservation equation allowing to model the purely conductive heat transfer within the tunnel lining and the surrounding ground reads:

$$\rho c_p\frac{\partial T}{\partial t} + \lambda\nabla^2 T = 0 \tag{5}$$

where ρc_p [J/(m³°C)] and λ [W/(m°C)] are the volumetric heat capacity and the effective thermal conductivity of the considered material (i.e., reinforced concrete or ground), respectively. While the volumetric heat capacity and thermal conductivity of the heat carrier fluid circulating in the pipes are considered to vary with temperature, those of the other materials characterising the investigated problem are considered to be insensitive to temperature changes.

The previous equations are solved for the pressure , the velocity $\bar{v}_{f,i}$ [m/s] and the temperature of the heat carrier fluid $\bar{T}_f$ [°C], and are coupled to the temperature field T [°C] obtained from the conductive–convective heat transfer equations solved for the pipes in the tunnel lining and the ground surrounding the tunnel. Currently, no experimental validation of the capability of the considered equations to capture the thermo-hydraulic behaviour of energy tunnels is available. However, these equations have been extensively applied to the modelling of the thermo-hydraulic behaviour of other energy geostructures, such as energy piles (Rotta Loria and Laloui, 2016; Rotta Loria and Laloui, 2018) and energy walls (Di Donna et al., 2017). Therefore, as long as appropriate hypotheses are employed, the considered equations are suitable to model the thermo-hydraulic behaviour of energy tunnels, with the capability to describe situations that are likely to be encountered in practice with adherence to reality.

2.4. Boundary and initial conditions

A schematic of the model boundary and initial conditions is presented in Fig. 3. A symmetry boundary is considered on the vertical surface crossing the 2 m-wide ring and the surrounding ground, meaning that no heat flux occurs across this boundary (boundary condition of the second kind), i.e.:

$$-n_i\cdot(-\lambda\nabla T) = 0 \tag{6}$$

A constant temperature (boundary condition of the first kind) is applied to the far field boundaries of the model domain (i.e., on the top and bottom horizontal boundaries of the model as well as on the vertical surfaces on the sides of the model), where the heat exchanger segment influence is negligible and the temperature is thus equal to the initial temperature, i.e.,

$$T_\infty = T_0 \tag{7}$$

with T_0 = 13 °C (BRGM, 1977). This initial temperature is applied to all of the domains of the model.

Heat transfer at the interface between the tunnel and the inner tunnel environment is driven by convection resulting from the airflow over the concrete surface. Accounting for this phenomenon is paramount when no thermal insulation is applied to the tunnel wall for limiting the influence of the tunnel environmental conditions on the heat exchange (Bourne-Webb et al., 2016). The presence of convection heat transfer leads to an increase in the thermal power that can be harvested from energy geostructures compared to situations in which only conduction heat transfer would be involved. For this reason, convection heat transfer is considered in the analysis through the following boundary condition:

$$\dot{q}_{conv} = \bar{h}_c(T - \bar{T}_a) \tag{8}$$

where $\bar{h}_c$ [W/m²°C] is the daily weighted average (over the considered season) of the forced convection heat transfer coefficient characterising the considered problem and $\bar{T}_a$ [°C] is the average seasonal air temperature in the tunnel. A forced convection heat transfer coefficient of $\bar{h}_c$ = 15.13 W/(m²°C) is evaluated according to the relationship with

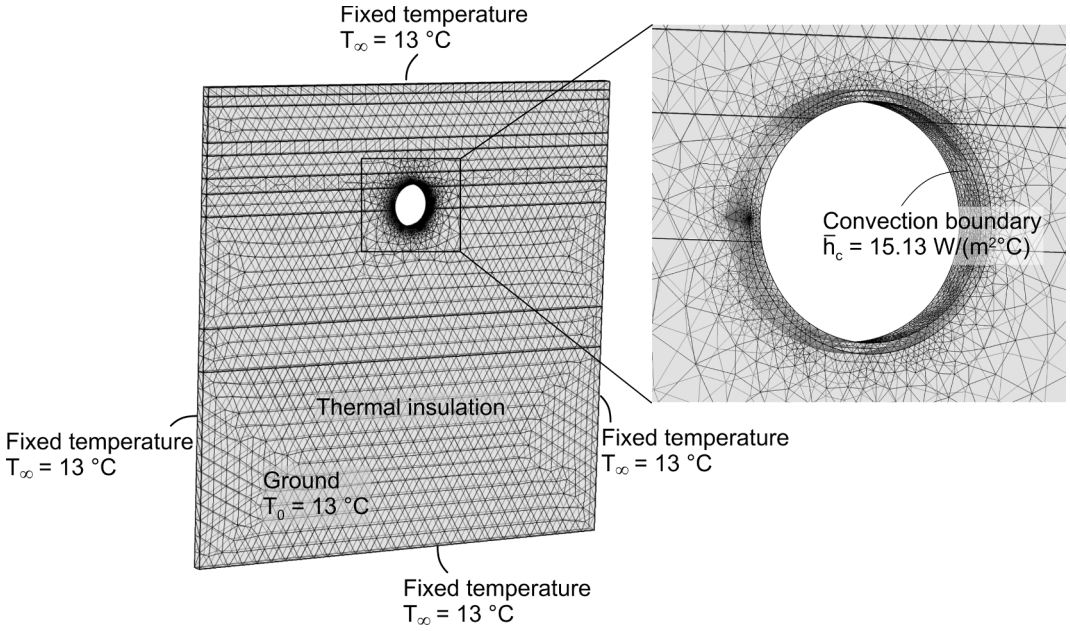

Fig. 3. Schematic of the finite element model boundary conditions.

the airflow velocity proposed by Lee et al. (2009). A train-induced unsteady airflow velocity that fluctuates throughout the day according to the train operation reported by Reinke and Ravn (2004) (peak-hour frequency, off-peak hour frequency, no operation) is calculated for the previous purpose. This unsteady airflow is characterised by velocity values that range between 1 m/s (design value of the ventilation system for this tunnel) and 5 m/s (peak value caused by piston effect of airflows in urban tunnels). A constant tunnel air temperature over time of $\bar{T}_a$ = 18.96 °C equal to the average temperature recorded in winter 2013 by the RATP (*Régie Autonome des Transports Parisiens*, i.e., the Parisian transports operator) in the tunnel of the Auber station is considered. The evolution with time of the reference temperature is shown in Fig. 4.

A constant inlet temperature of the heat carrier fluid circulating in the pipes of $\bar{T}_{in}$= 2 °C is imposed to maximise the heat exchange. The flow rate of the heat carrier fluid circulating in the pipes is subjected to a sensitivity analysis detailed in Section 2.6.

Considering constant values of temperature and convection heat transfer coefficient simulating the airflow in the tunnel as well as a constant trend of inlet temperature characterising the heat carrier fluid circulating in the pipes appears to be a meaningful and consistent approach with respect to the time-scale of the numerical simulations. In principle, all of the previous variables vary over time. In practice, simulations with constant yet representative input values of thermal loads, initial conditions and boundary conditions during relatively short time-scales allow achieving results under steady conditions that may be superimposed through Duhamel's principle. In this way, the response of the system for any different (e.g., more complex) thermal load can be achieved through the consideration of an appropriate number of simulation results in which constant unit-step loads that decompose the total load profile over time are considered.

Different numbers of elements characterise the mesh of the finite element models depending on the considered pipe configurations and embedment. Depending on the previous variables, the meshes include from 32,616 to 137,508 domain elements, from 8525 to 15,015 boundary elements, and from 1784 to 3413 edge elements.

Simulations are run for a time of t= 16 days, with the goal to achieve steady conditions. These conditions are considered to be reached when the difference of extracted thermal power is inferior to 0.5% compared to the one of the previous day. Such a criterion is fulfilled in all of the modelled cases after a time of t= 16 days. Results associated with steady conditions yield to the lower boundaries for the energy exploitation characterising the considered problem.

2.5. Material properties

The modelled soil layers are considered to be isotropic and fully saturated by water. Equivalent thermo-physical properties given by the fluid and the solid phases are taken from a local geological survey (Société du Grand Paris., 2016) and the Swiss Norm SIA 384/6 (SIA, 2010). These properties are reported in Table 1. The temperature sensitivity of the properties of the heat carrier fluid circulating in the pipes follows the expressions detailed in Table 1.

2.6. Investigated design solutions

To address the thermo-hydraulic behaviour and the related energy performance of energy segmental linings, the following design solutions are considered for given hydrogeological, geotechnical, geothermal,

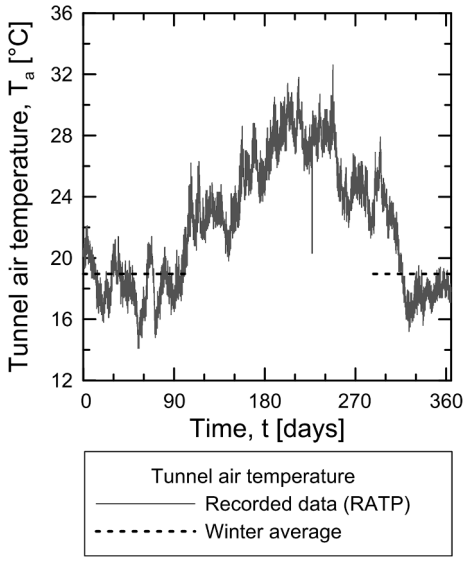

Fig. 4. Measured air temperature at the Auber station and winter average for the year 2013.

Table 1
Summary of the material parameters used in the numerical model.

Formation	λ [W/(m °C)]	c_p [J/(kg°C)]	ρ [kg/m³]
Backfill material	0.6	790	1900
Modern alluvium	1.4	1210	1900
Ancient alluvium	2.3	1260	1900
St − Ouen limestone	2.3	1333	1800
Beauchamp sand	2.3	1140	2100
Lower Marl	2.1	1100	2000
Coarse limestone	2.8	1050	2100
Upper sand	2.3	1140	2100
Concrete	1.8	880	2300
Water	= f(T) *	= f(T) **	= f(T) ***
HDPE pipe	0.35	–	–

* $f(T) = -0.869083936 + 0.00894880345 \cdot T - 1.5836634 \cdot 10^{-5} \cdot T^2 + 7.97543259 \cdot 10^{-9} \cdot T^3$
** $f(T) = 12010 \cdot 1471 - 80 \cdot 4072879 \cdot T + 0 \cdot 309866854 \cdot T^2 - 5 \cdot 3818688 \cdot 10^{-4} \cdot T^3 + 3 \cdot 62536437 \cdot 10^{-7} \cdot T^4$
*** $f(T) = 838 \cdot 466135 + 1 \cdot 40050603 \cdot T - 0 \cdot 0030112376 \cdot T^2 + 3 \cdot 71822313 \cdot 10^{-7} \cdot T^3$

Table 2
Considered pipe diameters and resulting pipe spacing.

Pipe diameter [mm]/pipe wall thickness [mm]	Pipe spacing [mm]
20/1.9	200
32/2.9	300

aerothermal and geometrical properties.

2.6.1. Pipe configuration

The influence of the pipe configuration is investigated by considering that pipes may be installed in tunnel energy segmental linings with a different layout and diameter. On the one hand, pipes may be installed following two layouts, i.e.: (1) parallel to the tunnel axis and (2) perpendicular to the tunnel axis. On the other hand, the upper and lower boundaries that characterise pipe diameters typically used for geothermal applications may be considered, i.e., (1) 32 mm and (2) 20 mm. Four pipe configurations result from the previous pipe diameters and pipe layouts, and are considered in this study, i.e., (1.1) 32 mm diameter pipes installed parallel to the tunnel axis, (1.2) 20 mm diameter pipes installed parallel to the tunnel axis, (2.1) 32 mm diameter pipes installed perpendicular to the tunnel axis, (2.2) 20 mm diameter pipes installed perpendicular to the tunnel axis. The rationale for considering the previous pipe configurations is that varying the pipe diameter involves changing the minimum pipe spacing and bending radius (Table 2), and thus the density of pipes per unit surface of tunnel lining. An example of this densification is illustrated in Fig. 5 with reference to the addressed pipe configurations.

2.6.2. Heat carrier fluid flow rate

The influence of the heat carrier fluid flow rate is examined for a variation of the average heat carrier fluid velocity at the inlet of the pipes, $\bar{v}_{in}$. The considered values of heat carrier fluid velocity are associated with typical Reynolds numbers that may be considered for geothermal applications, i.e.: 6000, 9000 and 12,000. The heat carrier fluid velocities corresponding to the different pipe diameters are detailed in Table 4. In the analyses, the Reynolds number is calculated as follows:

$$Re = \frac{\rho_f \bar{v}_{in} d_p}{\mu_f} \tag{9}$$

where $\rho_f = 1003$ kg/m³ and $\mu_f = 1.520 \cdot 10^{-3}$ kg/(m s) are the values of density and dynamic viscosity of the heat carrier fluid at the relevant temperature, respectively.

2.6.3. Pipe embedment

The influence of the distance between the pipes in the lining and the tunnel intrados (i.e., the pipe embedment) is investigated by considering that a minimum distance of 200 mm is often required to protect pipes from fire effects (Nicholson et al., 2014). To be representative for any thickness of tunnel linings, the pipe embedment is expressed in normalised form via the ratio between the distance from the intrados, s_i [mm], and the lining thickness, t_i [mm], i.e.: 0.5, 0.625 and 0.75. An example of the resulting locations of the pipes within the lining is illustrated in Fig. 6 with reference to limited portions of a cross-section of the lining that is perpendicular to the tunnel axis. It is considered that the influence of the pipe embedment on the total installed pipe length is compensated at the connection between the segment. Based on the previous consideration, the pipe variation associated with a change in the pipe embedment (a 60 cm difference in pipe length per ring characterises the solutions with the minimum and maximum pipe embedment) is neglected for the calculations. The same average value is

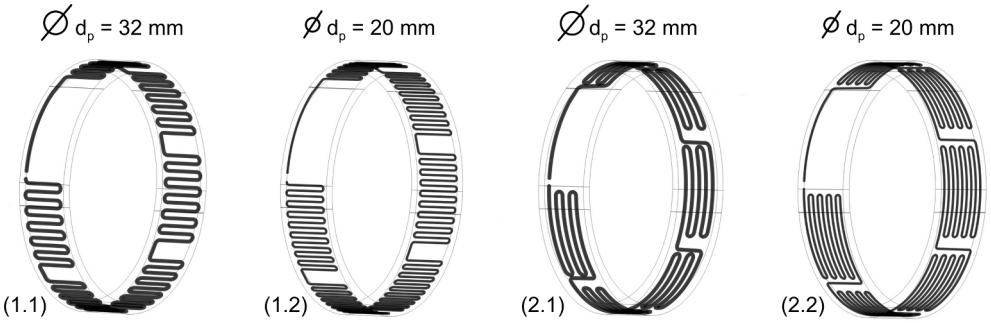

Fig. 5. Considered pipe configurations: (1.1) 32 mm diameter pipes parallel to the tunnel axis, (1.2) 20 mm diameter pipes parallel to the tunnel axis, (2.1) 32 mm diameter pipes perpendicular to the tunnel axis, (2.2) 20 mm diameter pipes perpendicular to the tunnel axis.

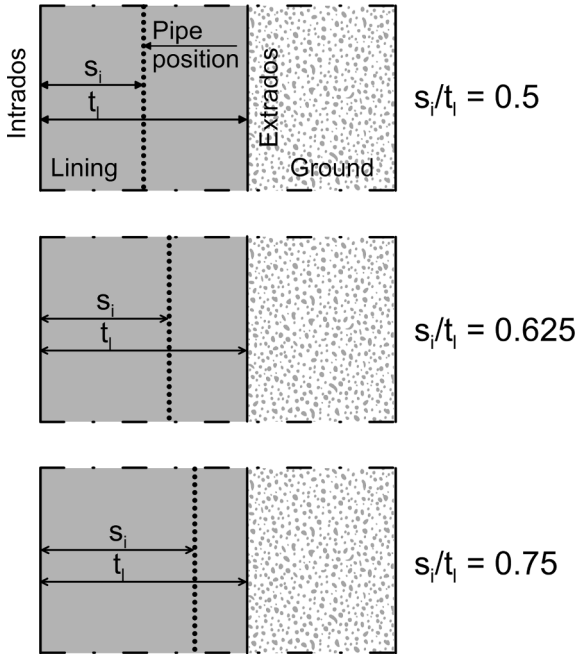

Fig. 6. Considered pipe embedment. The sketches represent portions of vertical cross-sections of the lining that are perpendicular to the tunnel axis.

considered for all solutions (see Table 3).

A summary of the considered design solutions is reported in Table 5. A total of 36 different possible energy segmental lining designs are investigated.

3. Influence of the design solutions on the energy performance

3.1. Harvestable thermal power

In the following, the energy performance of the modelled tunnel lining is compared for a variation of the analysed design solutions in terms of the extracted thermal power per unit surface. The extracted thermal power $\dot{Q}$ [W] can be computed as

$$\dot{Q} = \dot{m}_f c_{p,f}(\bar{T}_{out} - \bar{T}_{in}) \tag{10}$$

where the fluid mass flow rate in the pipes $\dot{m}_f$ [kg/s] is calculated considering the average value of ρ_f [kg/m^3] corresponding to the inlet and outlet temperatures $\bar{T}_{in}$ and $\bar{T}_{out}$, respectively ($\rho_f(T)$ according to Table 1), and the same applies to the specific heat of the heat carrier fluid $c_{p,f}$ [J/(kg°C)] ($c_{p,f}(T)$ according to Table 1). The resulting thermal power per unit surface of tunnel lining $\dot{q}_i$ [W/m^2] is calculated by dividing the extracted thermal power calculated via Eq. (10) by the modelled ring inner surface, i.e.:

$$\dot{q}_i = \frac{\dot{Q}}{w_{ring}\pi D_{in}} \tag{11}$$

where w_{ring} [m] is the ring width.

Fig. 7 shows the extracted thermal power per unit surface of tunnel lining for the investigated design solutions. The results show that the chosen design solutions have a significant influence on the energy performance of energy segmental linings. A 49% variation between the lowest and highest value of extracted thermal power can be observed. Installing smaller diameter pipes perpendicular to the tunnel axis, increasing the heat carrier fluid flow rate and decreasing the pipe embedment are ways to improve the energy performance of energy segmental linings. The influence of these design solutions on the energy performance are detailed in the following with respect to each other.

Fig. 8 shows the temperature distribution in the tunnel lining and the surrounding ground for the four different pipe configurations (considering the average pipe embedment $s_i/t_l = 0.625$ and the average Reynolds number Re= 6000) after 16 days of operation. The pipe configuration influences the ground temperature distribution and the thermal power that is harvested from the ground. A local heating of the ground by the tunnel air is observed behind the key segment. This phenomenon occurs because the key segment is only equipped with a straight pipe (to simplify the manufacturing process) and allows the heat to propagate from the tunnel to the ground more easily compared to the regions of the lining in which a relatively high density of thermally active pipes is encountered. The most significant disturbance of the ground temperature field as a consequence of the geothermal operation of the modelled tunnels is observed within the first metre from the extrados of the geostructure.

3.2. Pipe configuration

Fig. 9 shows the average extracted thermal power per unit surface of tunnel lining for the four considered pipe configurations after 16 days of operation, including the variation of the considered variable depending on the remaining design solutions (Reynolds number and pipe embedment). Among the four pipe configurations considered, the configuration involving the smaller diameter pipes installed perpendicular to the tunnel axis yields to the greatest pipe length per segment and represents the optimal solution in terms of extracted thermal power

Table 4
Considered values of average heat carrier fluid velocity at the inlet of pipes for different pipe diameters and Reynolds numbers.

Pipe diameter [mm]	**Reynods number [−]**		
	6000	9000	12000
	Heat carrier fluid velocity [m/s]		
20	0.50	0.75	1.00
32	0.31	0.47	0.62

Table 5
Overview of the analysed design parameters.

Parameter	**Value**
Pipe layout	Layout 1; Layout 2
Pipe diameter [mm]/pipe spacing [mm]	32/300; 20/200
Reynods number [−]	6000; 9000; 12000
Pipe embedment [−]	0.5; 0.625; 0.75

Table 3
Installed pipe length for the different configurations (average pipe embedment $s_i/t_l = 0.625$).

Pipe configuration	**Pipe length per segment [m]/pipe length per ring [m]**
1.1	21.1/134.5
1.2	32.9/192.1
2.1	19.6/121.7
2.2	34.1/207.8

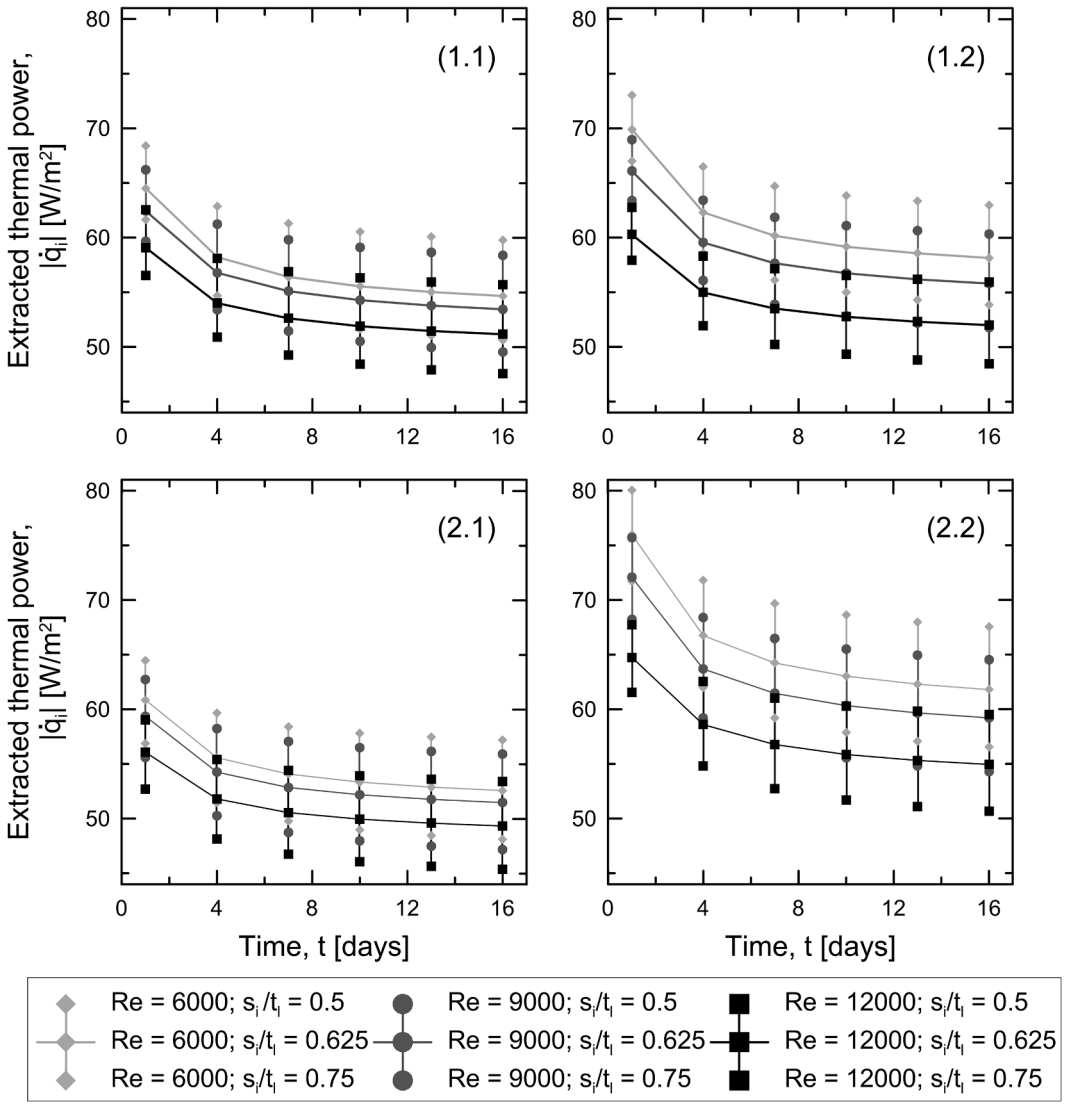

Fig. 7. Extracted thermal power per unit of tunnel lining surface for all the 36 design solutions over 16 days: (1.1) 32 mm diameter pipes installed parallel to the tunnel axis, (1.2) 20 mm diameter pipes installed parallel to the tunnel axis, (2.1) 32 mm diameter pipes installed perpendicular to the tunnel axis, (2.2) 20 mm diameter pipes installed perpendicular to the tunnel axis.

per unit surface of tunnel lining. Numerical results corroborating the previous evidence are given in Table 6, along with the percentage increase of extracted thermal power calculated with respect to the minimum reference value corresponding to configuration 2.1. Installing larger diameter pipes leads to a higher yield of thermal power per meter of pipe, despite a smaller pipe length per ring is installed. A 38% variation of extracted thermal power is observed when installing the pipes parallel to the tunnel axis, while a 49% variation is remarked when installing the pipes perpendicular to the tunnel axis. However, the previous approach does not represent the optimal design solution from a strictly energy performance-related point of view. For the same pipe diameter but a different pipe configuration, the pipe length influences the heat extraction rate. This influence can be assessed from Table 6 by comparing the pipe configurations 1.1 and 2.1 as well as 1.2 and 2.2, under the assumption that the orientation of the pipes with respect to the tunnel axis does not influence the harvested thermal power. For a 10.5% difference in length between the pipe configurations 1.1 and 2.1, a 4.5% difference in extracted thermal power per ring is observed. For an 8.2% difference in length between the pipe configurations 1.2 and 2.2, a 6.5% difference in extracted thermal power per ring is observed.

3.3. Heat carrier fluid flow rate

Fig. 10 shows the extracted thermal power per unit surface of tunnel lining after 16 days of operation with the configuration 2.2 installed, considering three different flow rates and three different pipe embedment. Increasing the Reynolds number enhances the convection heat transfer between the heat carrier fluid and the surrounding environment, thus minimising the convection heat transfer resistance in the pipes. This influence increases with a decreasing pipe embedment, because reducing the spacing between the pipes and the tunnel intrados reduces the conduction thermal resistance of the concrete lining. The energy performance improvement achieved by increasing the fluid flow rate increases less markedly for a successive increase of the Reynolds number because it reduces the heat exchanger effectiveness. The percentage of extracted thermal power variation with varying flow rates are provided in Table 7 for the considered pipe embedment. Increasing the mass flow rate of the fluid circulating in the pipes markedly improves the energy performance. This improvement decreases as the Reynolds number (and thus the mass flow rate) is increased by 50% and 100%.

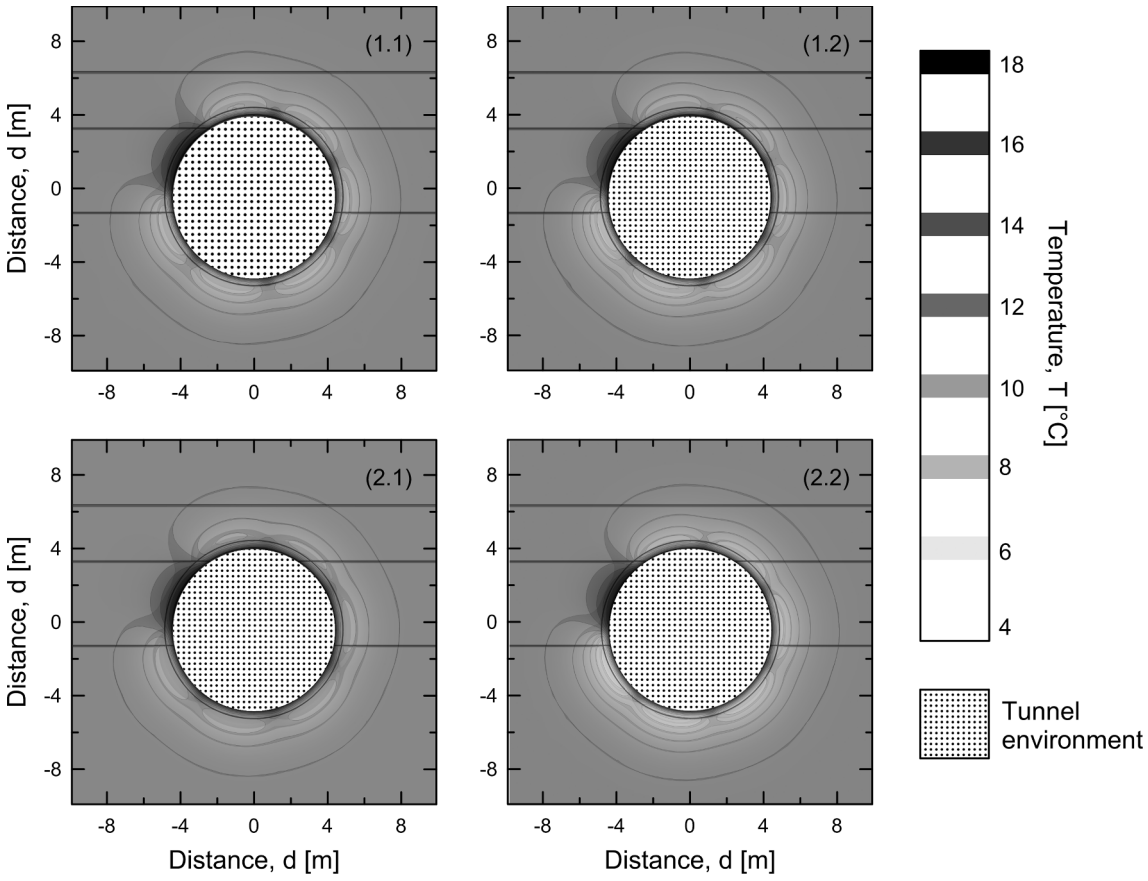

Fig. 8. Temperature distribution in the tunnel lining and the surrounding ground for the four considered pipe configurations (s_i/t_l = 0.625 and *Re* = 6000) after 16 days: (1.1) 32 mm diameter pipes installed parallel to the tunnel axis, (1.2) 20 mm diameter pipes installed parallel to the tunnel axis, (2.1) 32 mm diameter pipes installed perpendicular to the tunnel axis, (2.2) 20 mm diameter pipes installed perpendicular to the tunnel axis.

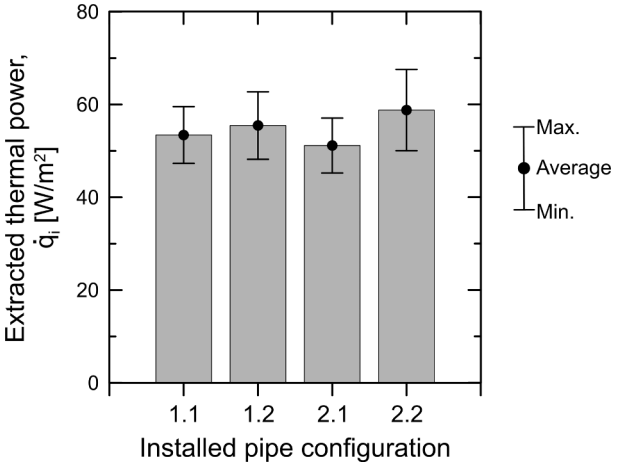

Fig. 9. Average extracted thermal power for 4 different pipe configurations after 16 days: (1.1) 32 mm diameter pipes installed parallel to the tunnel axis, (1.2) 20 mm diameter pipes installed parallel to the tunnel axis, (2.1) 32 mm diameter pipes installed perpendicular to the tunnel axis, (2.2) 20 mm diameter pipes installed perpendicular to the tunnel axis.

3.4. Pipe embedment

Fig. 11 shows the extracted thermal power per unit surface of tunnel lining after 16 days of operation with the configuration 2.2 installed, considering three different values of pipe embedment and three different flow rates. Reducing the pipe embedment facilitates the conduction heat transfer between the heat carrier fluid and the tunnel air, thus minimising the conduction heat transfer resistance of the lining. This influence increases with a successive decrease of the pipe embedment and an increase of the Reynolds number, because the latter reduces the convection thermal resistance in the pipes. The percentages of extracted thermal power variation for a change in the pipe embedment are provided in Table 8 for the considered Reynolds numbers. Decreasing the pipe embedment markedly improves the energy performance. This improvement increases as the pipe embedment is reduced by 1/6 and 1/3.

4. Influence of the design solutions on the economic attractiveness

4.1. General

In the following, the performance of a thermal power plant resorting to an energy segmental lining is assessed for the first time from the perspective of the economic attractiveness. The relevance of this type of analyses is that, although the energy performance of a tunnel segmental lining equipped as a heat exchanger may be enhanced through specific design solutions among those described in the previous sections, the economic attractiveness of the application and the possible influence of the energy geostructure design on the latter has yet to be demonstrated. This demonstration is typically paramount to justify the benefit of installing energy geostructures instead of conventional geostructures as well as to provide evidence for the savings involved with reference to other technologies harvesting renewable energies.

The economic attractiveness of any application can be determined via a detailed analysis of the costs and the profitability. In the context of thermal power plants resorting to energy geostructures, the costs

Table 6
Influence of the pipe configuration on the extracted thermal power after 16 days.

Configuration	1.1	1.2	2.1	2.2
Average extracted thermal power per ring [W]	2920	3032	2796	3214
Extracted thermal power per unit of lining surface [W/m^2]	53	55	51	59
Configuration influence (with respect to minimum) [%]	+ 4.43	+ 8.44	–	+ 14.95
Extracted thermal power per metre length of pipe[W/m]	22	16	23	15

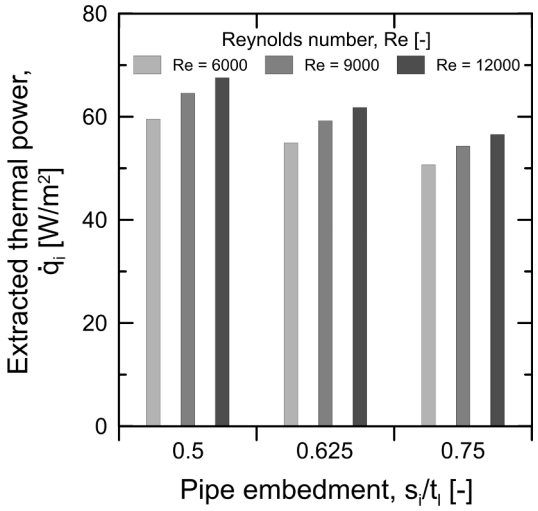

Fig. 10. Extracted thermal power with the configuration 2.2 installed for three considered flow rates and three considered pipe embedment after 16 days.

Table 7
Influence of the Reynolds number on the extracted thermal power after 16 days - configuration 2.2.

Pipe embedment [−]	Reynolds number [−]	
	6000 → 9000	6000 → 12000
0.5	+ 8.43%	+ 13.46%
0.625	+ 7.76%	+ 12.46%
0.75	+ 7.18%	+ 11.59%

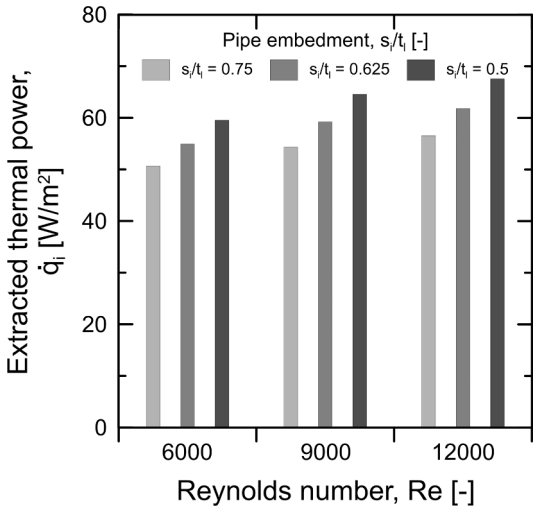

Fig. 11. Extracted thermal power with the configuration 2.2 installed for three considered pipe embedment and three considered flow rates after 16 days.

Table 8
Influence of the pipe embedment on the extracted thermal power after 16 days - configuration 2.2.

Reynolds number [−]	Pipe embedment [−]	
	0.75 → 0.625	0.75 → 0.5
6000	+ 8.45%	+ 17.48%
9000	+ 9.04%	+ 18.85%
12000	+ 9.30%	+ 19.46%

comprise the capital investment and operating costs related to the implementation and operation of the thermal power plant. They depend on the design of the plant and determine the cost of the supplied energy (also called levelized cost of energy, LCOE). For a given energy market situation, the profitability results from the ability of incomes resulting from the costs involved to yield a suitable return on investment.

Based on the consideration of the previous aspects, a new design methodology for energy geostructures targeting economic-related objectives is reported in Fig. 12. This methodology is detailed thereafter for an application of a thermal power plant resorting to an energy segmental lining.

4.2. Cost analysis

4.2.1. Capital investment

The capital investment comprises the additional initial costs involved in the implementation of the thermal power plant. These costs can be derived from a market analysis and include the following contributions:

Pipes and fittings: depend on the pipe diameter and are typically reported in the technical documentation provided by the producers, along with the investment cost for the piping tools. An additional 5% may be considered for the pipe costs to account for installation off-cuts.
Pipe support mesh: depends on the presence of an existing support for the pipes in the concrete. An additional support mesh could typically be necessary in the case of fibre reinforced concrete used for the lining segments, as no steel cage would be present.
Manual labour: results from the local hourly labour cost and the time required to equip the energy geostructure.
Header pipes: depend on the pipe diameter and are typically reported in the technical documentation provided by the producers. The required diameter for the inflow and return header pipes results from the fluid flow rate and the number of pipe circuits connected in parallel. The cost for the header pipes must consider the eventual additional length required for a distribution network (see next point).
Distribution network: comprises the civil work for the required length of district network to connect the thermal power plant to the energy users.
Heat pump fleet: results from the extracted thermal power and is typically reported in the technical documentation provided by the producers, along with the fees for the installation and commissioning.
Circulation pumps: results from the required pumping power, calculated from the critical loop head losses detailed in Section 4.2.2.

In the context of this study of a thermal power plant resorting to an energy segmental lining, the considered pipe configurations and heat carrier fluid flow rates result from the energy performance analysis. As reducing the pipe embedment improves the energy performance of the energy segmental lining without influencing the costs, the minimum pipe embedment (s_l/t_l = 0.5) is considered as reference design solution. The influence of the possible use of fibre reinforced concrete for the

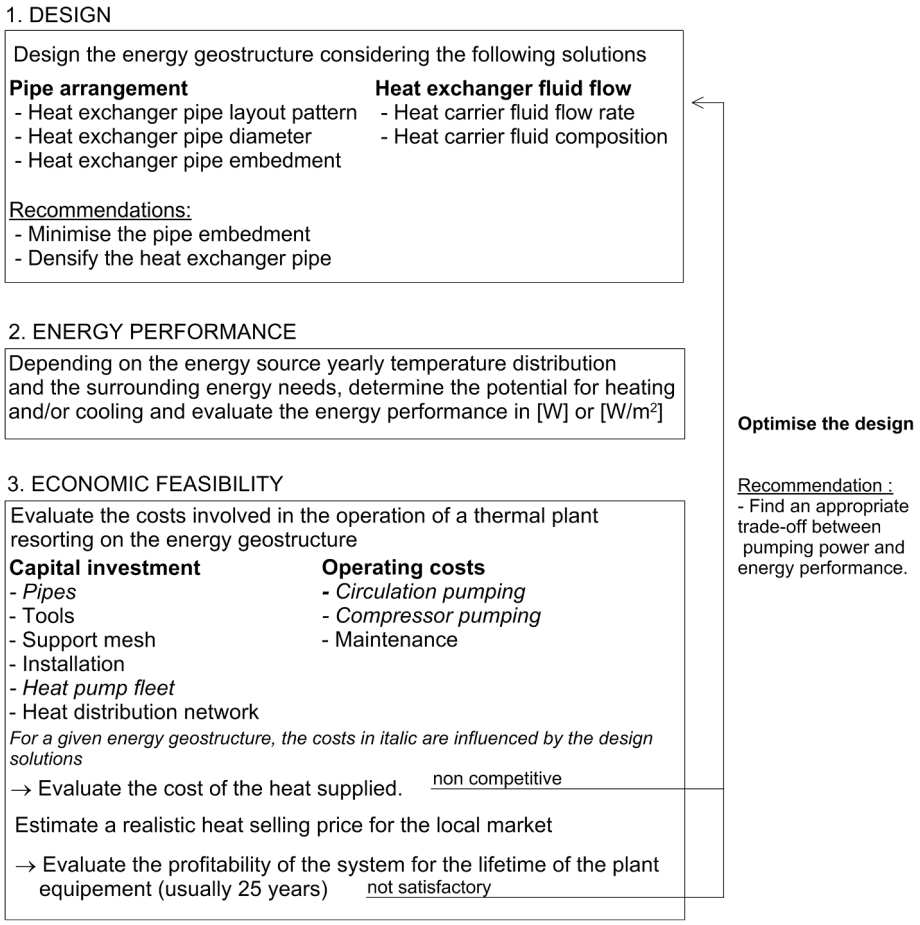

Fig. 12. Economic oriented design process for energy geostructures.

lining segments is investigated. The economic consequence of equipping variable tunnel lengths (200 m or 300 m) is also examined, while an average 100 m-long distribution network is considered for all the design solutions. A unique circulation pump is considered, corresponding to the one providing the largest required pumping power among every possible design. Because of the high temperature levels characterising the tunnel during the cooling season (Fig. 4), using the energy segmental lining for cooling purposes is not considered.

4.2.2. Operating costs

The operating costs comprise the regular costs resulting from the operation of the thermal plant. These costs include the following contributions:

Circulation pumping: results from the total hydraulic head losses in the so-called critical pipe loop, i.e., the pipe connecting the most hydraulically remote point of the system to the pump. The total hydraulic head losses H_{tot} [m] are distributed between the Moody-type friction losses (computed for the length of pipes) and the so-called local losses (associated with flow disruption due to the pipe configuration or plumbing components such as pipe bending, tee junctions, control valves) (Kudela, 2012). These losses are calculated as follows:

$$H_{tot} = \sum L_{pipe} h_{f,pipe} + \sum n_k h_{L_k} \tag{12}$$

where L_{pipe} [m] is the length of the considered pipe (header or heat exchanger pipe) and $h_{f,pipe}$ [m/m] is the linear friction loss per metre length of this pipe (provided by the pipe producers in the form of pressure loss tables) n_k [−] is the number of considered flow disturbance (pipe bending, tee junctions, control valves) and h_{L_k} [m] is the local loss associated with the disturbance. The latter term can be calculated for each disturbance as follows:

$$h_{L,k} = K_{L,k} \frac{\bar{v}_f^2}{2g} \tag{13}$$

where $K_{L,k}$ [−] is a dimensionless local loss coefficient depending on the considered pipe component and g [m/s²] the gravitational constant.

The required pumping power $\dot{P}_{pump}$ [W] resulting from the previous total head losses can be computed as:

$$\dot{P}_{pump} = \frac{1}{\eta_{pump}} H_{tot} \dot{V}_f \rho_f g \tag{14}$$

where η_{pump} [−] is the pumping efficiency and $\dot{V}_f$ [m³/s] is the fluid volumetric flow rate. The yearly pumping costs $c_{pump,yr}$ [EUR] can finally be calculated as:

$$c_{pump,yr} = \dot{P}_{pump} t_{op,yr} c_{el} \tag{15}$$

where $t_{op,yr}$ [hrs] is the yearly reference operational time of the thermal power plant and c_{el} [EUR/kWh] is the local electricity price.

Heat pump compressor pumping: results from the following power balance for the thermal power plant:

$$\dot{Q}_{source} = \dot{Q}_{supplied} - \dot{E}_{input} \tag{16}$$

where $\dot{Q}_{source}$ [W] is the extracted thermal power from the energy source, $\dot{E}_{input}$ [W] is the electrical power input used by the heat pump compressor and $\dot{Q}_{supplied}$ [W] is the thermal power supplied to the consumer. This latter term can be calculated as:

Table 9
Levelized cost of energy for the analysed design solutions.

Configuration	Equipped length [m]					
	200			300		
	Reynolds number [−]					
	6000	9000	12000	6000	9000	12000
	Levelized cost of energy [EUR/kWh]					
1.1	0.0863	0.0901	0.0928	0.0906	0.0947	0.1069
1.2	0.0779	0.0795	0.0867	0.0781	0.0852	0.0856
2.1	0.0872	0.0912	0.0941	0.0917	0.0944	0.1088
2.2	0.0765	0.0801	0.0846	0.0782	0.0833	0.0835

$$\dot{Q}_{supplied} = \frac{COP}{COP - 1}\dot{Q}_{source} \tag{17}$$

where COP [−] is the coefficient of performance of the heat pump defined as the ratio between the electrical power input $\dot{E}_{input}$ [W] and the supplied thermal power $\dot{Q}_{supplied}$ [W]. The COP varies depending on the available source temperature and the required supplied temperature, and is typically reported in the technical documentation provided by the producers.

Depending on the energy geostructure design and the resulting supplied power, the cost of the electrical power input for the heat pump compressor $c_{HP,yr}$ [EUR/year] is finally computed as:

$$c_{HP,yr} = \frac{\dot{Q}_{supplied}}{COP} t_{op,yr} c_{el} \tag{18}$$

Maintenance: The yearly maintenance cost for the heat pump fleet typically takes the form of a support and maintenance subscription arranged by the producers. No maintenance is required for the piping.

In the context of this study of a thermal power plant resorting to an energy segmental lining, the header pipe diameter is chosen according to recommended head loss limitations, so that a higher mass flow rate (resulting from a longer installed length or a higher Reynolds number) results either in a higher pumping power (thus pumping cost), or in a larger, thus more expensive header pipe. As previously mentioned, a unique type of circulation pump is considered, with an efficiency $\eta_{pump} = 0.7$. The required yearly thermal plant operation is of $t_{op,yr} = 2880$ hrs/year to provide both space heating and domestic hot water during the heating season (operating 12 hrs per day) and domestic hot water only for the rest of the year (operating 4 hrs per day). $\dot{Q}_{source}$ [W] is computed as:

$$\dot{Q}_{source} = \dot{q}_i \pi D_{in} l_{equipped} \tag{19}$$

where $\dot{q}_i$ [W/m^2] is the extracted thermal power per unit surface of tunnel lining according to the results of the energy performance analysis and $l_{equipped}$ [m] is the tunnel equipped length. Because the source temperature does not markedly vary during seasons in energy tunnel applications, a yearly-constant COP= 3.5 is considered according to a supplier literature review, corresponding to the provision of hot water at 55 °C from source water at 7 °C.

4.2.3. Levelized cost of energy

The adopted design solutions can be compared in terms of their levelized cost of energy, which is a widespread method to benchmark different energy production systems. The LCOE gives the average price that should be paid by consumers to accurately repay the investor (or operator) for the capital and operation, with a rate of return equal to the discount rate. This parameter is calculated in [EUR/kWh] as follows:

$$c_{heat} = \frac{A_{yr} + Op_{yr}}{Q_{supplied}} \tag{20}$$

where Op_{yr} [EUR] are the yearly operation costs, $Q_{supplied}$ [kWh] is the yearly supplied energy and A_{yr} [EUR] is the annuity of the investment costs that can be calculated as

$$A_{yr} = I_0 \frac{i(1+i)^n}{(1+i)^n - 1} \tag{21}$$

with I_0 [EUR] the total initial investment calculated before, i [%] the discount rate and n [−] the relevant period of time in years. The discount rate allows the harmonisation of present and future values by converting the future incomes into annualised costs at present value. It reflects the expected rate of return demanded by investors depending on different dimensions such as the investor's forward-thinking and alternative investment opportunities, as well as the risk of an investment opportunity comprising the policy-induced, country-specific and technology-related risks (Steinbach and Staniaszek, 2015).

In the context of this study of a thermal power plant resorting to an energy segmental lining, it is assumed that the entire amount of energy extracted from the energy segmental lining is sold. Therefore, the yearly supplied energy can be computed as:

$$Q_{supplied} = \dot{Q}_{supplied} t_{op,yr} \tag{22}$$

Considering a favourable political atmosphere, reasonable technological risks and a local renewable energy discount rate analysis, a discount rate value of $i = 6\%$ is considered. In addition, although a tunnel is supposed to operate for at least 80 years, the number of years $n = 25$ considered for the economic evaluation corresponds to the lifespan of most of the tunnel and thermal plant equipment (ventilation, heat pump, circulation pump, etc.). The reason for this choice is that many parameters used in the previous calculations may change after the previous period of time because of the substitution of technological components of the plant that may be characterised by a lower cost and involve a greater mechanical efficiency. Therefore, a longer analysis may lead to misleading results.

4.3. Profitability

The profitability is assessed through the calculation of the net present value, i.e., the present value of the investment and discounted future incomes (resulting from the costs involved) over the considered lifetime of the project. The net present value NPV [EUR] is calculated as:

$$NPV = -I_0 + \sum_{t=0}^{n} \frac{C_t}{(1+i)^t} \tag{23}$$

where C_t [EUR] is the yearly cash flow calculated as the income resulting from the involved costs to which the operation costs are deducted. The income cash flow comprises the regular earnings resulting from the operation of the thermal power plant. This includes the sale of the extracted energy as well as eventual additional effects on the infrastructure such as the possible ventilation savings in energy tunnel applications where the energy extraction will decrease the tunnel air temperature and subsequently the tunnel ventilation requirements.

In the context of this study of a thermal power plant resorting to an energy segmental lining, a local heat selling price of 120 EUR/MWh for a newly installed thermal power plant is considered. Quantifying the ventilation savings would require enabling the existing tunnel heat and ventilation design to be revised to include the energy segmental lining and is considered out of the scope of this work.

4.4. Methodology application

The LCOE [EUR/kWh] calculated for the design solutions considered

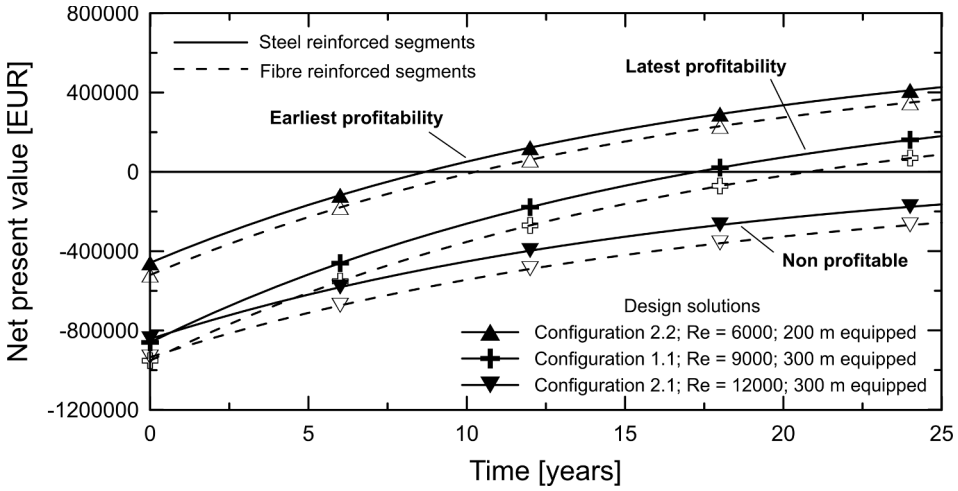

Fig. 13. Net present value over 25 years for the design solutions leading to earliest and latest investment profitability, and non-profitable ones, with the offset related to the use of fibre reinforced segment.

Table 10
Return on investment after 25 years for four different pipe configurations and two different tunnel equipped lengths with a given flow rate (Re = 6000).

	200 [m] equipped			
Configuration	1.1	1.2	2.1	2.2
NPV after 25 years [EUR]	245858	380466	221968	427094
ROI after 25 years [%]	146	185	143	193
	300 [m] equipped			
Configuration	1.1	1.2	2.1	2.2
NPV after 25 years [EUR]	269236	565885	233402	597765
ROI after 25 years [%]	132	188	128	190

in this study is reported in Table 9. It appears that the design solutions markedly influence the cost of the supplied energy. The following considerations about the economic attractiveness of thermal power plants resorting to energy segmental linings can be identified:

For every possible heat exchanger design, selecting a greater pipe diameter systematically induces a higher LCOE because this solution limits the densification of the heat exchanger segment and leads to marked flow rates and head losses.
For a given pipe configuration, increasing the flow rate results in a higher LCOE. This is attributed to the fact that the increased pumping power or header pipe cost (in the case of a necessary increase of the diameter) are not compensated by the subsequent greater extracted thermal power and resulting heat sale.
For a given equipped length and flow rate, installing smaller diameter pipes perpendicular to the tunnel axis allows to extract the highest thermal power and leads to a lower LCOE.

The cheapest supplied heat (in bold in Table 9) is achieved when installing pipes according to configuration 2.2 on a 200 m-long tunnel section, leading to a LCOE of 7.65 cts/kWh.

In case of fibre reinforced segments, the addition of a support steel mesh in the heat exchanger segment leads to higher investment costs (+11.5% on average) and thus a higher LCOE (+5.2% in average).

The net present value for the design solutions leading to earliest and latest profitability, as well as the non-profitable ones, are presented in Fig. 13, with the offset related to the eventual use of fibre reinforced segment. The profitability, which is related to the LCOE, shows great variability. The lower the LCOE is, the earlier the profitability of the investment (NPV = 0EUR) will be. Therefore, the energy segmental lining design leading to the lower LCOE is profitable after 8.5 years of operation (after 10 years with fibre reinforced segments). The energy segmental lining designs leading to the highest LCOE are profitable after 17 years (21 years with fibre reinforced segments) or even non-profitable over 25 years. This result highlights that the chosen energy segmental lining design can strongly jeopardize its economic attractiveness while presenting, at least in principle, an acceptable energy performance.

The investment yield may also be assessed trough the calculation of the return on investment, ROI, after 25 years. As shown in Table 10, the NPV after 25 years is influenced by the equipped length and increases significantly for a given pipe configuration when installing smaller diameter pipes (35% higher on average). The higher ROI (in bold in Table 10) is achieved with the design solutions leading to the cheapest supplied heat.

5. Concluding remarks

This work presents the first comprehensive analysis of the energy performance and economic attractiveness of energy segmental linings for subway tunnels. To address the first aspect, the work provides information on the influence of a wide range of design solutions related to the pipe configuration and the features of fluid circulation on the energy performance. To address the second aspect, the work investigates the economic consequences of the investigated design solutions on the costs and profitability of thermal power plants resorting to the investigated technology. The proposition and application of a methodology to address the economic attractiveness of thermal power plants resorting to energy geostructures such as tunnels, with reference to the features of this study, demonstrates that while the energy performance of energy segmental linings may be significantly enhanced when adopting given design solutions, the most efficient design does not lead to the lowest LCOE and the earliest profitability.

Every energy geostructure has to be designed based on its specific conditions. However, based on the results of this study, the following design approaches appear to be particularly effective for achieving a satisfactory energy performance and economic attractiveness of energy segmental linings: (i) Densify the heat exchanger segment with smaller diameter pipes whenever possible (unless continuous energy supply is expected, due to the negative influence of potential and progressive thermal interactions between excessive closely spaced pipes); (ii) Apply a moderately turbulent flow rate to trade-off between high heat exchange and acceptable pumping power; (iii) Reduce the pipe embedment (when providing heating in the case of hot tunnels or cooling in the case of cold tunnels); (iv) Equip several times shorter tunnel

sections. While energy segmental linings may be highly competitive compared to other technologies harvesting renewable energy, a poor design can jeopardize the energy performance and economic attractiveness of such applications.

References

Barla, M., Di Donna, A., 2018. Energy tunnels: concept and design aspects. Undergr. Space 3 (4), 268–276.

Barla, M., Di Donna, A., Perino, A., 2016. Application of energy tunnels to an urban environment. Geothermics 61, 104–113.

Bidarmaghz, A., Narsilio, G.A., 2018. Heat exchange mechanisms in energy tunnel systems. Geomech. Energy Environ. 16, 83–95.

Bourne-Webb, P.J., Freitas, T.B., da Costa Gonçalves, R.A., 2016. Thermal and mechanical aspects of the response of embedded retaining walls used as shallow geothermal heat exchangers. Energy Build. 125, 130–141.

BRGM. (1977). Étude de la température des nappes peu profondes à Paris et dans la banlieue nord.

COMSOL Multiphysics Reference Manual, version 5.3.

Di Donna, A., Barla, M., 2016. The role of ground conditions on energy tunnels' heat exchange. Environ. Geotech. 3 (4), 214–224.

Di Donna, A., Cecinato, F., Loveridge, F., Barla, M., 2017. Energy performance of diaphragm walls used as heat exchangers. Proc. Instit. Civil Eng.-Geotech. Eng. 170 (3), 232–245.

Frodl, S., Franzius, J.N., Bartl, T., 2010. Design and construction of the tunnel geothermal system in Jenbach. Geomech. Tunnel. 3 (5), 658–668.

IEA, 2013. Transition to sustainable buildings, strategies and opportunities to 2050. International Energy Agency, Paris.

Kudela, H., 2012. Hydraulic losses in pipes. Wroclas University of Science.

Lee, Y., Choi, M.S., Yi, S.T., Kim, J.K., 2009. Experimental study on the convective heat transfer coefficient of early-age concrete. Cem. Concr. Compos. 31 (1), 60–71.

Peltier, M., Rotta Loria, A.F., Lepage, L., Garin, E., Laloui, L., 2019. Numerical investigation of the convection heat transfer driven by airflows in underground tunnels. Appl. Therm. Eng. https://doi.org/10.1016/j.applthermaleng.2019.113844.

Nicholson, D.P., Chen, Q., de Silva, M., Winter, A., Winterling, R., 2014. The design of thermal tunnel energy segments for Crossrail, UK. No. 3 In: Proceedings of the Institution of Civil Engineers-Engineering Sustainability. Thomas Telford Ltd, pp. 118–134.

Reinke, P., Ravn, S., 2004. Twin-tube, single-track high-speed rail tunnels and consequences for aerodynamics, climate, equipment and ventilation. HBI Haerter Ltd., Thunstrasse.

Rotta Loria, A.F., Laloui, L., 2016. Thermally induced group effects among energy piles. Géotechnique 67 (5), 374–393.

Rotta Loria, A.F., Laloui, L., 2018. Group action effects caused by various operating energy piles. Géotechnique 68 (9), 834–841.

SIA, Sondes Géothermiques, norme suisse 384/6, SN 546384/6 :2010 fr, Zurich (2010).

Société du Grand Paris. (2016). Lot 3 – Mémoire de synthèse géologique, hydrogéologique et géotechnique.

Steinbach, J., Staniaszek, D., 2015. Discount rates in energy system analysis. Fraunhofer ISI, Building Performance Institute Europe (BPIE): Karlsruhe, Germany.